





Original Article

# Influence of Distal Re-entry Tears on False Lumen Thrombosis After Thoracic Endovascular Aortic Repair in Type B Aortic Dissection Patients: A Computational Fluid Dynamics Simulation

DA LI,<sup>1</sup> TINGHUI ZHENG ,<sup>1</sup> ZHAN LIU,<sup>1</sup> YAN LI,<sup>1</sup> DING YUAN ,<sup>2</sup> and YUBO FAN<sup>3</sup>

<sup>1</sup>Department of Applied Mechanics, Sichuan University, Chengdu 610065, China; <sup>2</sup>Department Vascular Surgery of West China Hospital, Sichuan University, No. 37 Guo Xue Xiang, Chengdu 610041, China; and <sup>3</sup>Beijing Advanced Innovation Center of Biomedical Engineering, Key Laboratory for Biomechanics and Mechanobiology of Ministry of Education, School of Biological Science and Medical Engineering, Beihang University, Beijing 100191, China

(Received 20 October 2020; accepted 5 March 2021; published online 25 March 2021)

Associate Editor Francesco Migliavacca oversaw the review of this article.

## Abstract

**Purpose**—Distal re-entry tears play a significant role in false lumen (FL) thrombosis, which will strongly affect the postoperative long-term survival of patients with type B aortic dissection (TBAD) after thoracic endovascular aortic repair (TEVAR). This study aimed to investigate the influence of a peculiar morphological parameter of the residual re-entry tears in TBAD patients after TEVAR on long-term FL thrombosis using the computational fluid dynamics.

**Methods**—Ideal population-based three-dimensional models of post-operative TBAD were established. Numerical simulation was performed to investigate the hemodynamic differences caused by different tear features, including the tear count, the maximum distance between tears, and the tear area.

**Results**—Although the low relative residence time (RRT) area did not change significantly when the tear distance was fixed, the area of oscillatory shear index (OSI) > 0.45 and endothelial cell activation potential (ECAP) > 1.5 decreased significantly with the tear count and area increased and a dramatic increase in blood flow into the FL was also observed. When tear count and total area were fixed, for each 10-mm increase in the maximum distance between tears, the area of low RRT in the FL increased significantly, while the average pressure difference increased by 10.85%.

**Conclusion**—The different morphology of the re-entry tears had different effects on the thrombosis-related hemodynamic parameters in FL following TEVAR. and the number of re-

entry tears was most crucial to the potential thrombosis in the post-TEVAR FL of TBAD patients.

**Keywords**—Type B aortic dissection, Hemodynamics, Thrombosis, TEVAR, Tears.

## INTRODUCTION

Acute type B aortic dissection (TBAD) is a severe cardiovascular disease in which the intima of the aorta is suddenly torn, causing blood flow within the layers of the blood vessel and separating the inner from the outer layer.<sup>23</sup> In general, aortic dissection involves more than one tear, and if aortic dissection is not treated promptly or rightly, it can lead to complications such as aortic dilatation, organ ischemia, aortic rupture, and even death.<sup>25,31,44</sup> Currently, thoracic endovascular aortic repair (TEVAR) is the preferred treatment options for complicated TBAD,<sup>9,22</sup> aiming to cover the proximal tears, prevent blood from entering the false lumen (FL), and expand the volume of the true lumen (TL), in order to restore the normal blood flow channel, promote vascular remodeling, and enhance the formation of FL thrombosis.<sup>8</sup> However, given the uniqueness of some tear locations and limited lengths of the stent, not all tears can be physically covered during TEVAR. As a result, many patients still have distal re-entry tears.

Address correspondence to Ding Yuan, Department Vascular Surgery of West China Hospital, Sichuan University, No. 37 Guo Xue Xiang, Chengdu 610041, China. Electronic mail: lidamail@qq.com, tinghui.zh@scu.edu.cn, bmeliuzhan@163.com, lileah2016@scu.edu.cn, yuanding@wchscu.cn, yubofan@buaa.edu.cn

Clinical studies pointed out that the distal re-entry tears play a significant role in the TL remodeling and FL thrombosis following TEVAR.<sup>21,35</sup> Especially, the tear count,<sup>3,7,34,37,40</sup> area, and maximum distance of re-entry tears were suggested to be the risk factors of incomplete thrombosis in the post-TEVAR FL.<sup>37,43</sup> However, due to the fact that the post-operative FL thrombosis is a multi-factor outcome, it is difficult to perform systematic comparisons between patients. Moreover, because clinical statistics is greatly affected by the sample size, different sample sizes may lead to different analysis results. For example, Zhang et al.<sup>43</sup> found that the large maximum distance between re-entry tears would enlarge the FL and keep patent in FL, which would result in bad long-term complications. However, Ab Naim et al.<sup>37</sup> considered that large distances would be prone to thrombosis in FL.

Hemodynamics is well known to play an important role in thrombus formation.<sup>1,19</sup> Moreover, the computational fluid dynamics (CFD) method was reported to capture flow features, wall shear stress-related indices,<sup>32</sup> and pressure distribution,<sup>5</sup> which contribute to the initiation and development of thrombosis but these features are difficult to measure clinically. While there have been a lot of hemodynamic analysis on post-operative TBAD using patient-specific models<sup>11,12,30</sup> which greatly help us to understand the mechanism of thrombosis formation in the FL following TEVAR. However, up to now, there has been no systematic investigation on the impact of the re-entry tear morphology on the FL thrombosis, and the individual impact of a particular tear parameter remains poorly understood.

It is a common practice in cardiovascular research to adopt an idealized geometry to qualitatively capture and reflect the essence of the investigated problem.<sup>4,41</sup> An idealized geometry based on the data analysis of human anatomies represents the commonness of different human bodies can capture the main features and properties of the structure and ignore their individuality.<sup>4</sup> Moreover, an idealized model makes it possible to change one specific morphology feature at a time while keeping the other factors constant. Such models will help identify if and to which extent a specific factor promotes the impaired hemodynamics.

Therefore, this study aimed to investigate the different influence of the morphology parameters of residual re-entry tears on the tendency to thrombus formation in the FL of TBAD after TEVAR. In particular, the influence of tear count, area, and maximum distance between tears on local flow features will be analyzed by CFD on population-based idealized three-dimensional (3D) models.

## METHODS

### *Establishment of Ideal Models*

Based on the clinical observation and previous studies, both the ascending aorta and the aortic arch have a degree of distortion which exists in three dimensions.<sup>17,36</sup> Therefore, the ideal aorta models not only contained the main branch of the aorta, the true and false lumen but also took into consideration the angulation of the aortic arch and the tortuosity of descending aorta (Fig. 1d).

Also, the parameters of re-entry tears in 48 patients were measured. These parameters were measured by CT images within one week after TEVAR. The flow chart of these patients was mentioned in our previous research.<sup>16</sup> The Ethical Review Committee of the West China Hospital of Sichuan University approved this research. Because this was a retrospective study, the requirement of obtaining informed consent was waived. Among them, the average tortuosity of descending aorta was 0.05, the average area of each tear was 18 mm<sup>2</sup>, the average maximum distance between the re-entry tears was 40 mm, the average number of re-entry tears was 2.8.

Finally, the ideal curved 3D model of the TBAD aorta after TEVAR consisted of an ascending aorta inlet and eight outlets including the innominate artery, left carotid artery, left subclavian artery, celiac artery, superior mesenteric artery, right renal artery, left renal artery and abdominal aorta (Figs. 1a, 1b and 1c), and the diameters of inlet and outlets were based on the previous literature.<sup>41</sup> In addition, the false lumen is enclosed and connected to the true lumen through the tears.<sup>20</sup>

Specifically, in group A (Fig. 1a), the total area of the re-entry tears (36 mm<sup>2</sup>) and the maximum distance between re-entry tears (40 mm) were kept the same for all models. And the number of re-entry tears was set to be 2, 3, 4, and 5, which are all located in the major branches of the abdominal aorta.

In group B (Fig. 1b), the total number of re-entry tears and the total area of re-entry tears (36 mm<sup>2</sup>) were kept the same for all models. And the maximum distance between re-entry tears was set to be 10, 20, 30, 40, 50, and 60 mm.

In group C (Fig. 1c), the number of re-entry tear (2) and the location of the re-entry tear were kept the same for all models. And the area of each re-entry tear was set to be 18, 23, 28, 33, and 38 mm<sup>2</sup>.

To make a fair comparison, the morphology of TL and FL was the same in all models. And the shape of the tears was simplified into a circle to eliminate the interference of shape. The first re-entry tear in all models was located 114 mm from the aortic bifurca-

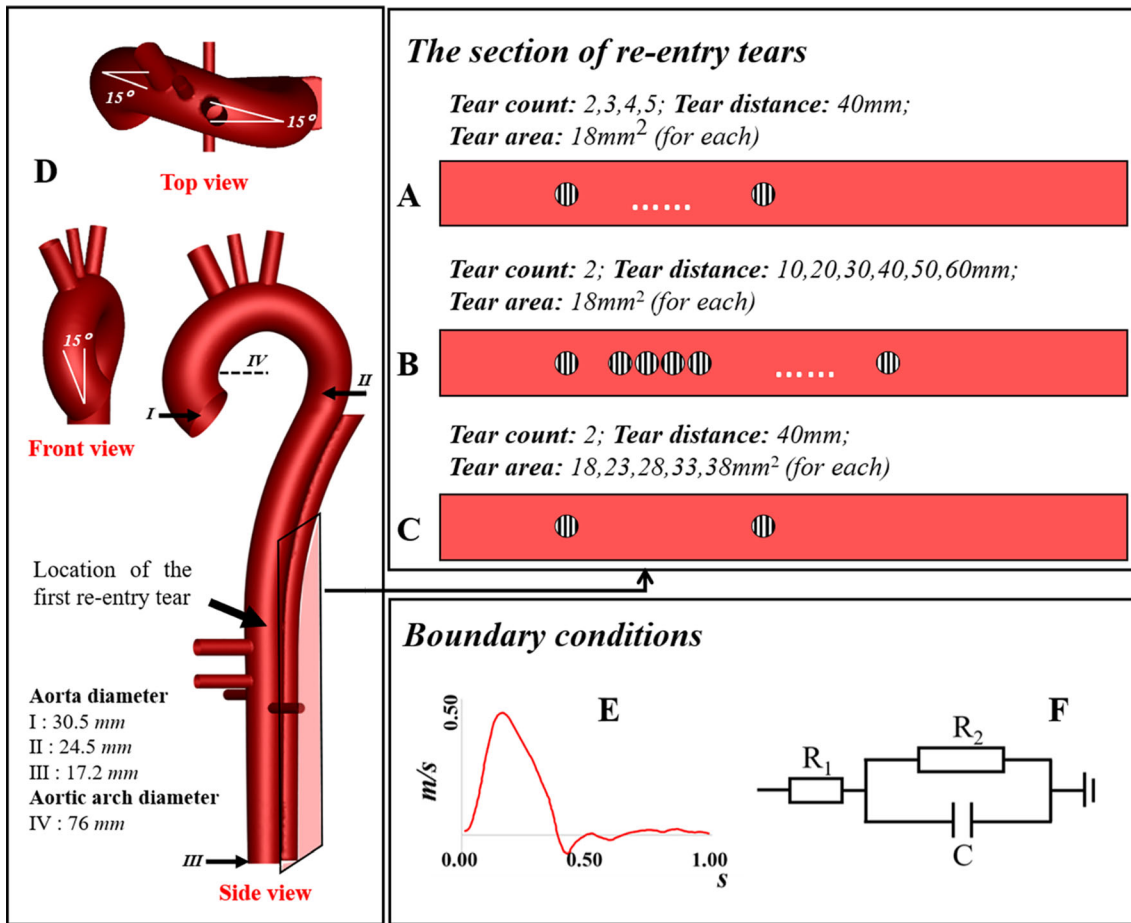


**FIGURE 1.** Establishment of the idealized model after thoracic endovascular aortic repair and the setting of boundary conditions. (Detailed aorta angulation and diameter was showed in D; A, B, and C represent sections between the true and false lumen and the tear parameters of the different groups)

tion, which was obtained from the average distance from the celiac trunk artery to the iliac artery in 48 patients.

### Hemodynamic Analysis

Blood flow was assumed isotropic, homogeneous, incompressible, and Newtonian, and the corresponding governing equations are given as follows:

$$\rho((\partial \vec{u})/\partial t + \vec{u} \cdot \nabla \vec{u}) + \nabla p - \mu \nabla \wedge 2\vec{u} = 0 \quad (1)$$

$$\nabla \cdot \vec{u} = 0 \quad (2)$$

where  $\vec{u}$  and  $p$  represent the fluid velocity vector and pressure, respectively.  $\rho$  and  $\mu$  are the density and dynamic viscosity of blood given to 1050 kg/m<sup>3</sup> and 3.5 × 10<sup>-3</sup> kg/m s, respectively.

A velocity waveform at the inlet of the ascending aorta as taken from the literature<sup>20</sup> was set on the inlet of all models, and the outlet adopted a three-element Windkessel model.<sup>29</sup> In the three-element Windkessel

model, the human circulatory system could be represented by the electrical circuit with three parameters  $R_1$ ,  $R_2$ , and  $C$  which represents the proximal resistance of the aorta, the resistance of peripheral vessels and the compliance of aortic walls respectively. The pressure of outlets was obtained with the following equation<sup>20</sup>:

$$P = (R_1 + R_2)Q - R_2C \frac{dP}{dt} + R_1R_2 \frac{dQ}{dt} \quad (3)$$

Since the ideal model was used in this study, the parameters of  $R_1$ ,  $R_2$ , and  $C$  of all models were adjusted by matching the velocity waveform of previous research until the systolic and diastolic pressures reached 120/80mmHg through a Python code using the methods in the literature.<sup>2</sup>

A rigid wall assumption and no-slip boundary condition were assumed. In this study, ICEM (ANSYS, Inc., Canonsburg, PA, USA) was used for mesh generation in all models, with a mixture of tetrahedral and prism volume meshes. The boundary layer had an element of 0.005 mm adjacent to the wall, progressively

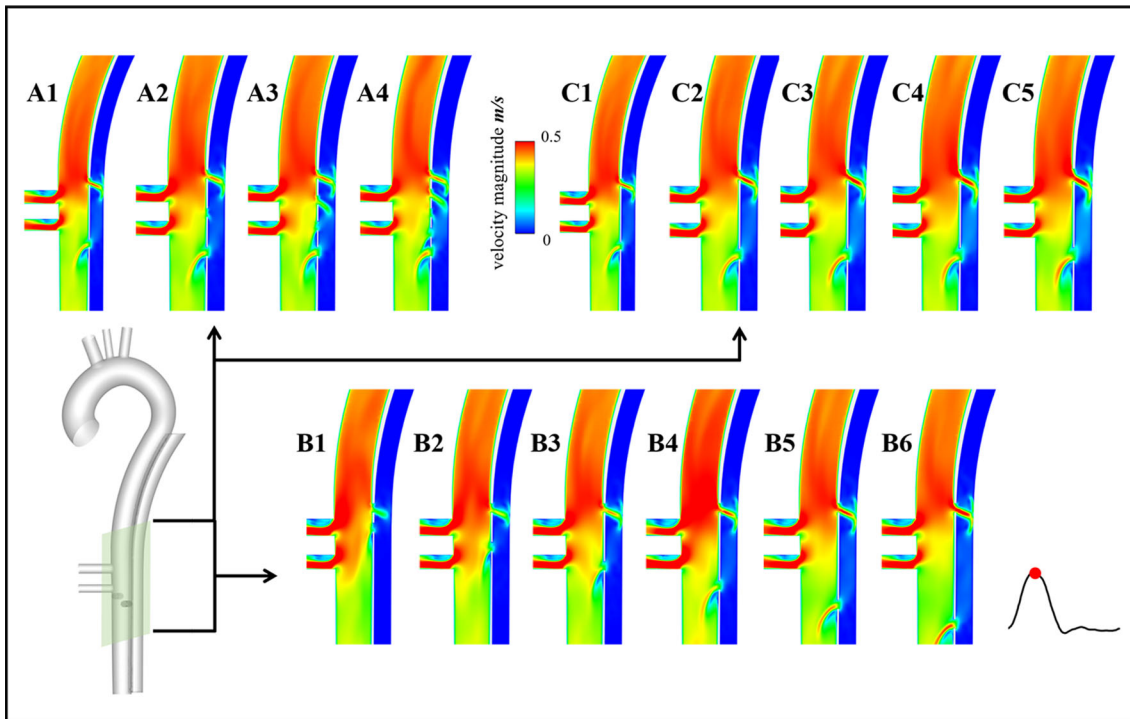


**FIGURE 2.** Flow field in three groups. (A1 = two re-entry tear; A2 = three re-entry tears; A3 = four re-entry tears; A4 = five re-entry tears; B1 = distance in 10 mm; B2 = distance in 20 mm; B3 = distance in 30 mm; B4 = distance in 40 mm; B5 = distance in 50 mm; B6 = distance in 60 mm; C1 = each area in 18 mm<sup>2</sup>; C2 = each area in 23 mm<sup>2</sup>; C3 = each area in 28 mm<sup>2</sup>; C4 = each area in 33 mm<sup>2</sup>; C5 = each area in 38 mm<sup>2</sup>)

growing over 10 layers to a total thickness of 1.1 mm. The number of elements of a mesh ranged from 487568 to 495510 in these 15 models. The average differences in the time-averaged wall shear stress (TAWSS) distribution between the standard and refined meshes were less than 1% under steady conditions, and more details were present in the supplementary material (supplementary material Table 1).

Flow visualization and analysis were completed by the CFD software (ANSYS FLUENT 12.0, ANSYS, Inc., Canonsburg, PA, USA) based on the finite volume method. A default implicit 3D solver was applied. Discretization of the equations involved a second-order upwind differencing scheme; SIMPLEC was adopted for the pressure velocity correction, and the residual error convergence threshold was set as  $10e-7$ . The pulse cycle was divided into 1000 times step sizes of 1 ms that  $T = 1$  s was the simulated cycle time. After the cycle-to-cycle simulation, the fifth cycle was considered to be stable, and the fifth cycle was selected for further analysis.

Parameters of flow fields, TAWSS, oscillatory shear index (OSI), relative residence time (RRT), and endothelial cell activation potential (ECAP) counter maps and pressure difference were visualized. Among them, OSI is a parameter that quantifies the magnitude of the wall shear stress and direction changes, and high

OSI will cause the blood to flow back and forth, resulting in endothelial cell damage, and finally forming intimal hyperplasia<sup>39</sup>; RRT is an index that can indicate the residence time of blood cell near the vessel wall,<sup>28</sup> and it is used to describe the relative residence time of blood flow and to reveal the site where blood flow is relatively easy to stop<sup>28</sup>; ECAP characterizes the possibility of thrombus formation.<sup>14</sup> The proportion of the area of  $RRT < 1 = \text{area of } RRT < 1 / \text{area of FL}$ . Pressure difference = average pressure of the TL—average pressure of the FL at the same section. TAWSS, OSI, ECAP, and RRT were defined as follows:

$$\text{TAWSS} = \frac{1}{T} \int_0^T |\text{WSS}| dt \quad (4)$$

$$\text{OSI} = 0.5 \left[ 1 - \frac{\left| \int_0^T \text{WSS} dt \right|}{\int_0^T |\text{WSS}| dt} \right] \quad (5)$$

$$\text{ECAP} = \frac{\text{OSI}}{\text{TAWSS}} \quad (6)$$

$$\text{RRT} = \frac{1}{(1 - 2\text{OSI})\text{TAWSS}} \quad (7)$$

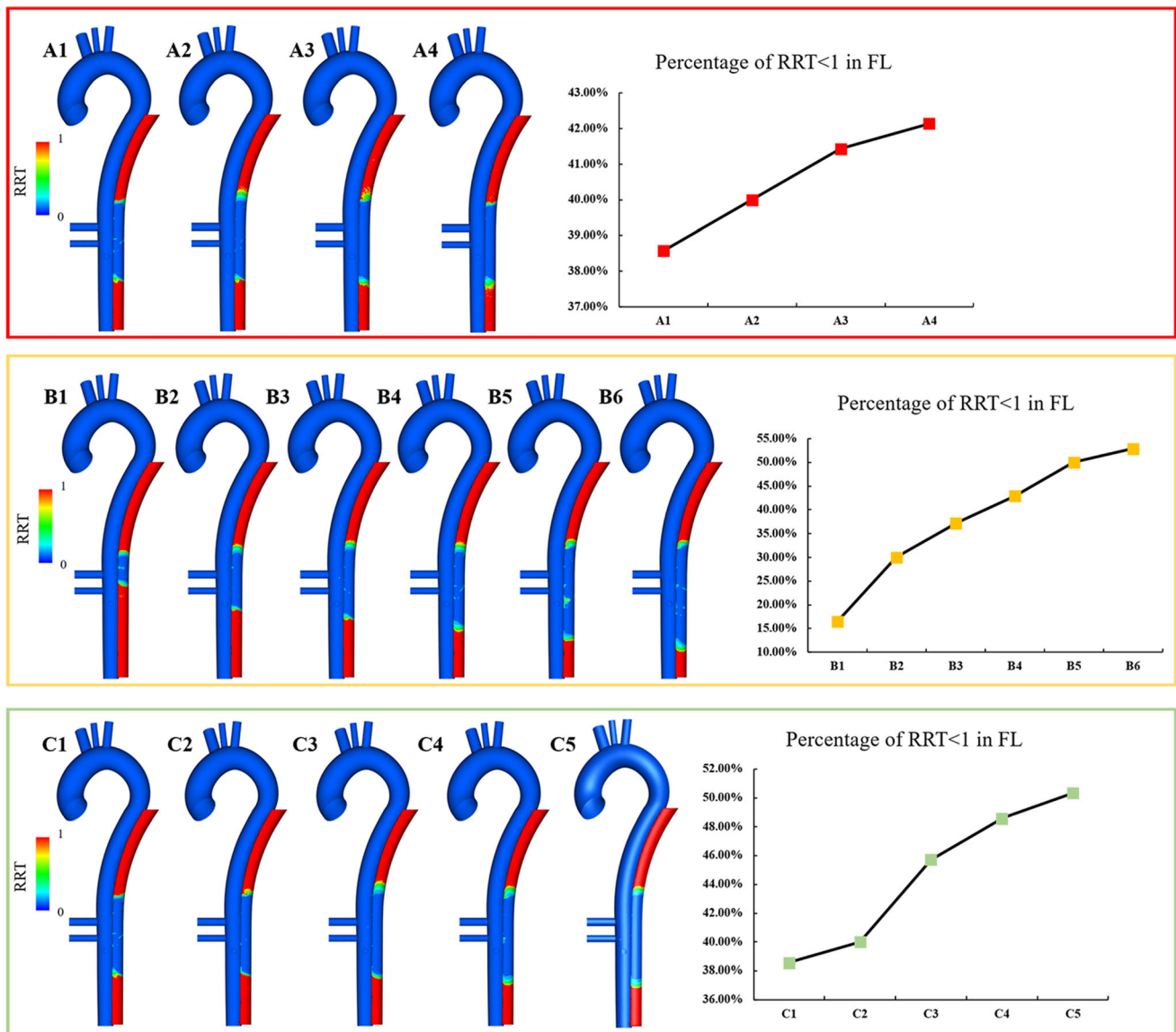


FIGURE 3. Relative residence time (RRT) maps and proportion of the area of RRT < 1 in three groups

## RESULTS

### *Influence of the Number of Re-entry Tears*

Given the same geometry of the TL, the flow field in the TL is similar (Fig. 2). However, with the increase in the number of re-entry tears, the blood flow field in the FL gradually became stable. At peak systolic, the jet flows that influenced the vessel wall of the FL was observed more intense with the increase of the re-entry tears (Figs. 2A1 and 2A4). Moreover, the area of RRT < 1 did not increase significantly with the increase in the number of re-entry tears (Figs. 3A1 and 3A4). The values of the area of RRT < 1 were 38.57%, 40.01%, 41.43%, and 42.14% respectively. However, the area of high OSI and high ECAP in the low RRT area in FL decreased rapidly. The values of the area of OSI >

0.45 (Figs. 4A1 and 4A4) were 25.01%, 15.99%, 6.04%, and 1.09% respectively. The values of the area of ECAP > 1.5 (Figs. 5A1 and 5A4) were 51.85%, 50.01%, 34.48%, and 28.81% respectively. Also, the low TAWSS area decreased significantly with the increase in the number of tears (Figs. 6A1 and 6A4). In addition, the pressure difference between the TL and FL did not change with the increase in the number of re-entry tears (Fig. 7a).

### *Influence of the Maximum Distance of Re-entry Tears*

With the increase in the maximum distance between re-entry tears, the flow field in the TL was similar, but the active area of the blood flow field in the FL increased obviously, and the blood flow in the FL

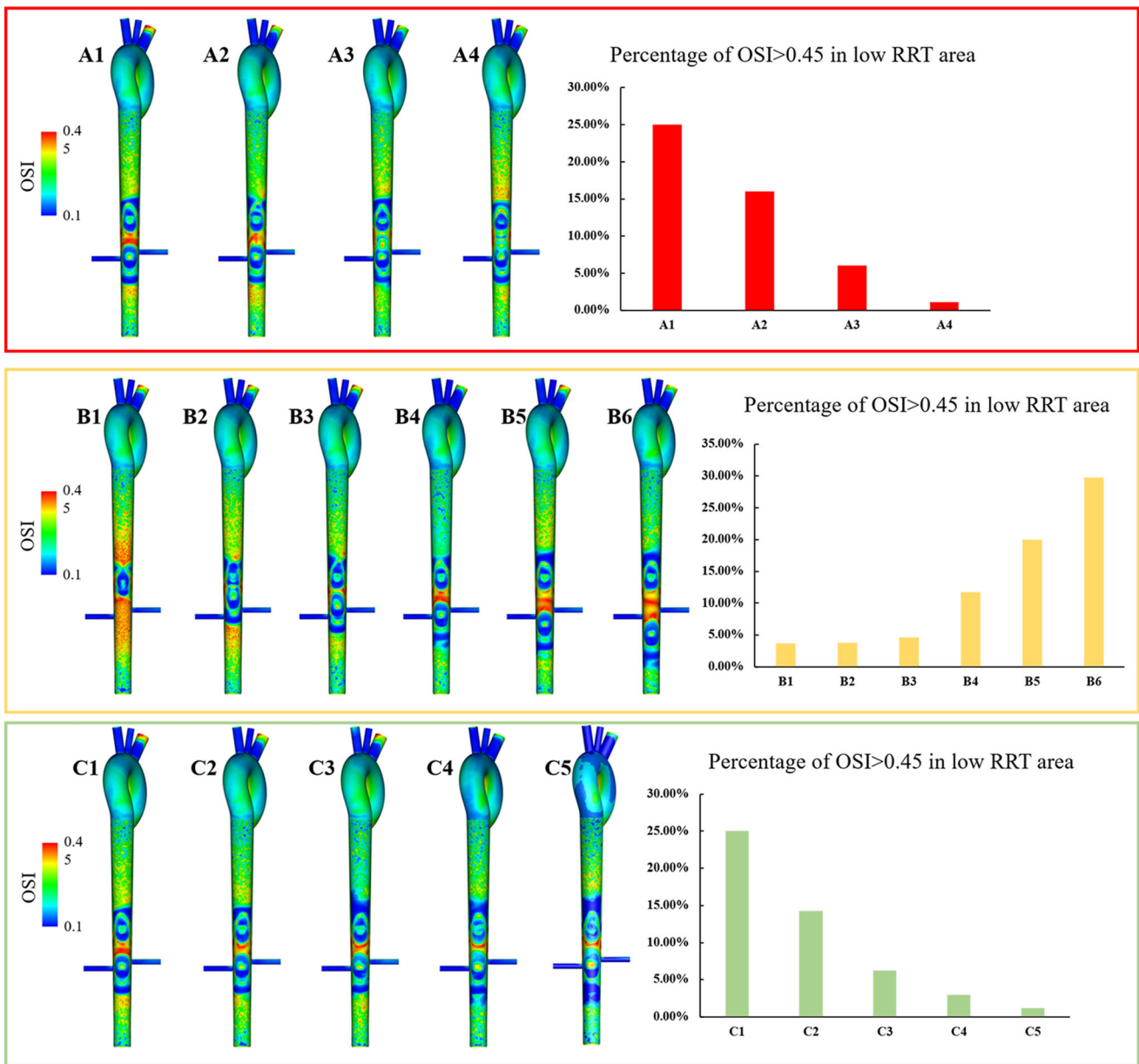


FIGURE 4. Oscillatory shear index (OSI) maps and the proportion of the area of OSI > 0.45 in three groups

gradually tended to be stable. Furthermore, the area of  $RRT < 1$  increased significantly, with values of 22.86%, 31.43%, 40.00%, 42.86%, 57.14% and 68.58%, respectively. However, the high OSI area and high ECPA area in the low RRT region in FL also increased significantly. Specifically, the values of the area of  $OSI > 0.45$  (Figs. 4B1 and 4B6) were 3.75%, 3.81%, 4.62%, 11.67%, 20.01% and 29.73% respectively. The values of the area of  $ECAP > 1.5$  (Figs. 5B1 and 5B6) were 21.74%, 47.62%, 53.85%, 58.33%, 62.86% and 64.05% respectively. The low TAWSS area was increased obviously between two re-entry tears. The pressure difference between the TL and FL gradually increased. Specifically, for every 10-

mm increase in the maximum distance, the average increase rate of the pressure difference is 10.85% (Fig. 7b).

#### *Influence of the Area of Re-entry Tears*

The flow field in the FL was disordered in all models (Figs. 2C1 and 2C5). However, with the increase of the re-entry tear area, the blood flow velocity increased significantly in the FL, and significant blood exchange was observed at the tear site of the C4 and C5 model. In addition, the area of  $RRT < 1$  increased smoothly. Compared with the 36-mm<sup>2</sup> model, the area of  $RRT < 1$  in the 46-mm<sup>2</sup> model increased by 20.13% and that

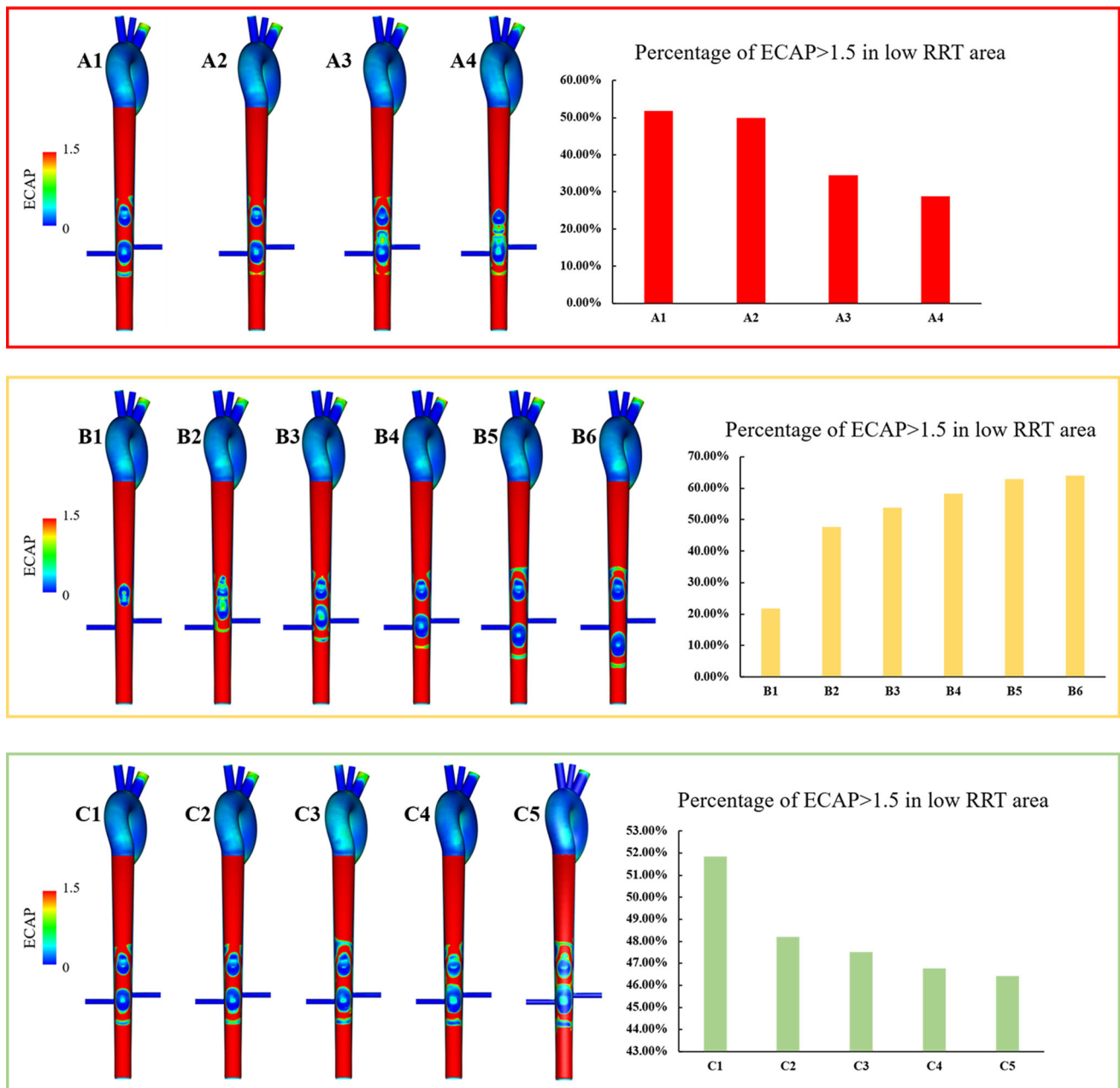


**FIGURE 5.** Endothelial cell activation potential (ECAP) maps and the proportion of the area of ECAP < 1.5 in three groups

in the 76-mm<sup>2</sup> model increased by 44.16%, with values of 42.78%, 51.39%, 54.17%, 58.33% and 61.67%, respectively. However, the area of high OSI and high ECAP in the low RRT area in FL decreased rapidly. The values of the area of OSI > 0.45 (Figs. 4C1 and 4C5) were 25.01%, 14.29%, 6.25%, 2.94% and 1.19% respectively. The values of the area of ECAP > 1.5 (Figs. 5C1 and 5C5) were 51.85%, 48.21%, 47.50%, 46.76% and 46.42%. Also, the low TAWSS area decreased significantly with the increase in the number of tears (Figs. 6C1 and 6C5). The pressure difference

between the TL and FL did not change significantly (Fig. 7c).

#### *Comparison of the Number, Maximum Distance and Area of Re-entry Tears*

Furthermore, this study quantified the effects of changes in the number, maximum distance and area of re-entry tears on different hemodynamic parameters to assess their effects on changing the hemodynamic environment in the FL (Table 1).

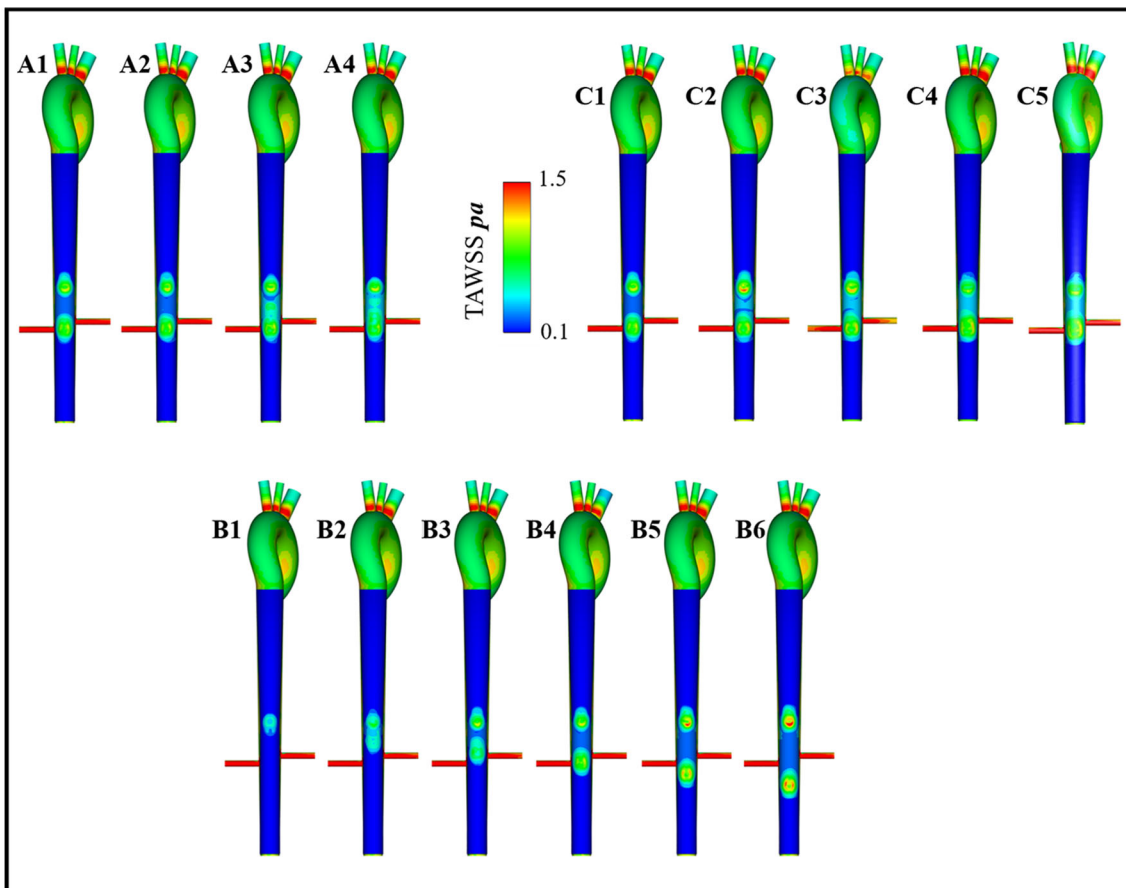


FIGURE 6. Time-averaged wall shear stress (TAWSS) maps in three groups

In the comparison of flow field changes between TL and FL, the most significant changes in the flow velocity and area of the jet flow into FL were observed in group C, and even a high-speed and stable flow channel was formed between the tears. However, models in group A mainly affected the area of the jet flow into the FL, while group B did not show any significant change in the area and velocity of the jet flow into the FL.

In the comparison of changes in the TAWSS related hemodynamic parameters in FL, for every 10 mm increase in the maximum distance between the re-entry tears, the  $RRT < 1$  area increased by 7.29% on average, the  $OSI > 0.45$  area increased by 7.19% on average and the  $ECAP > 1.5$  area increased by 8.46% on average. In addition, for every 10 mm<sup>2</sup> increase in the area of the re-entry tears, the  $RRT < 1$  area increased by 2.93% on average, the  $OSI > 0.45$  area decreased by 5.96% on average and the  $ECAP > 1.5$  area decreased by 1.35% on average. However, for every 1 increase in the number of re-entry tears, the  $RRT < 1$  area only increased by 1.19% on average, the  $OSI > 0.45$  area decreased by 7.97% on average

and the  $ECAP > 1.5$  area decreased by 7.68% on average.

## DISCUSSION

Outcomes of patients with TBAD are strongly related to aortic remodeling and FL thrombosis after TEVAR.<sup>13,25</sup> Continuous patency of blood flow in the FL will lead to a series of complications such as aortic expansion, collapse of the TL, and even rupture of the FL.<sup>24</sup> As re-entry tears are the only channel connecting the TL and FL, re-entry tears play a crucial role in the postoperative treatment effect of patients. In addition, hemodynamics has been widely acknowledged to predict thrombosis in FL.

The results revealed that all the morphologic features of re-entry tears including its count, maximum distance, and the area had an impact on the near wall and flow features in a FL following TEVAR. In addition, the tear count and the tear area had the greatest effect on the hemodynamic parameters related to thrombosis formation, especially the tear count. Specifically, when the maximum tear distance was



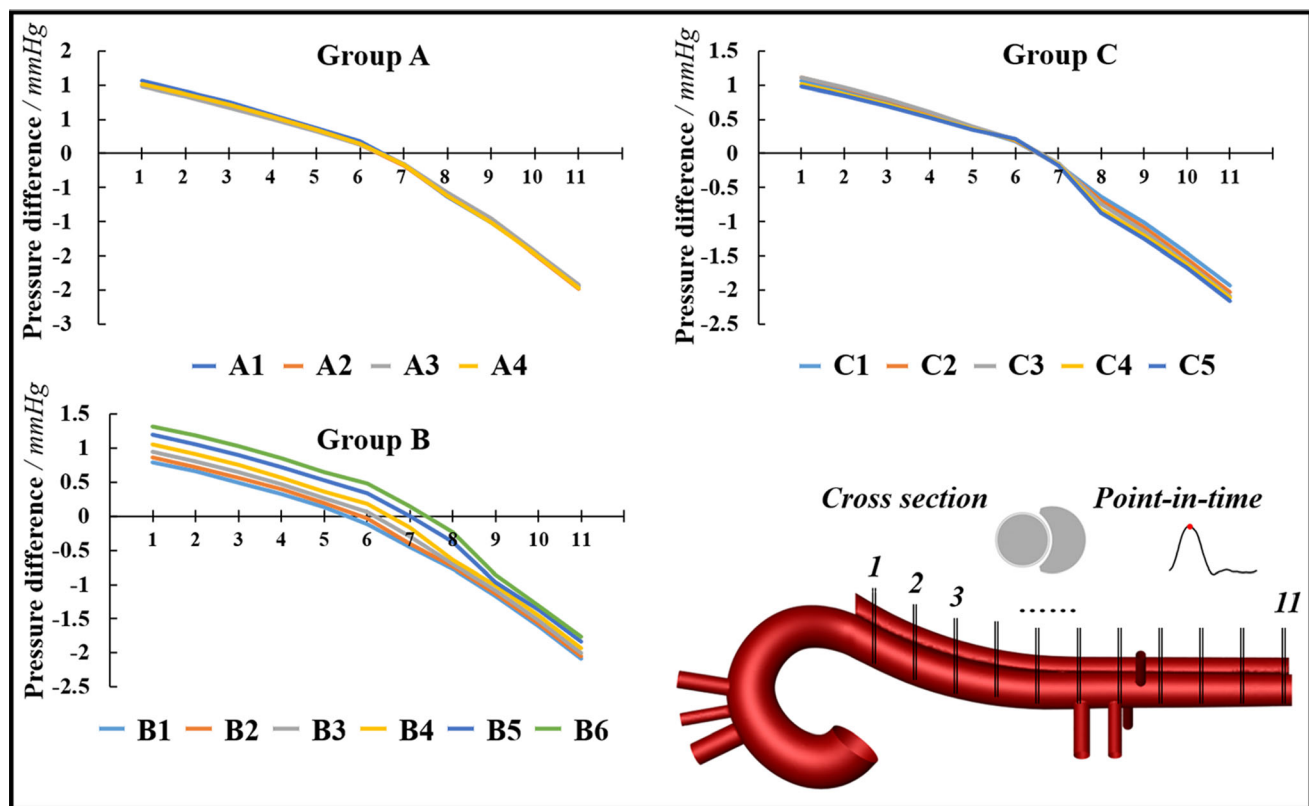


FIGURE 7. Pressure difference between the true and false lumen in three groups on 11 sections

fixed, the high OSI and the high ECAP regions between re-entry tears decreased dramatically with increasing tear count and area. The previous studies indicated that regions with high OSI and  $ECAP > 1.5$  were considered less prone to thrombosis,<sup>27,39,42</sup> which meant that the increase in tear count and tear area would prevent FL thrombosis in those areas. Moreover, areas with low TAWSS were generally considered to be more likely to develop thrombus.<sup>6,33</sup> In this study, it was found that low TAWSS area also dramatically decreased with the increase of tear count and area, also the TAWSS values between re-entry tears gradually became normal in the FL. Besides, the flow features in the FL experienced a significant change with the tear count increased, and each increase in the number of tears would increase the area of the high speed of jet flow into the FL, resulting in more fresh blood entering the FL during each cardiac cycle, maintaining the function of the blood channel in the FL and ultimately preventing thrombosis in the FL.

It was noted that when tear count and tear area fixed, increased maximum tear distance would lead to a significant increase in the low RRT area in the FL and the pressure difference between the true and false lumen. Regions with  $RRT < 1$  were considered less prone to thrombosis,<sup>10</sup> but previous studies suggested that a large pressure difference between TL and FL

would accelerate the blood exchange and prevent the blood from stagnating in the FL,<sup>12,38</sup> which can seriously prevent the formation of thrombus in the FL.<sup>20</sup> Moreover, the high OSI and high ECAP areas did not decrease with increasing tear distance, but increased significantly, suggesting that an excessively large maximum distance between re-entry tears could only lead to the formation of thrombus between tears.

In the current study, the tear parameters of the ideal model established were measured according to the real patients, it is reasonable to speculate that the common results reflected in the ideal model can be corresponding to the more complex real aorta. But it is worth noting that in a real case, an increase in the number of re-entry tears inevitably led to an increase in the total area of re-entry tears and even in some cases to an increase in the maximum distance of re-entry tears which will lead to an unfavorable hemodynamic environment for the initiation and formation of thrombosis, resulting in a decrease in the thrombosis rate in the FL following TEVAR. Accordingly, in order to increase the FL thrombosis, we suggest that the selective re-entry tears can be one-stage repaired following TEVAR based on tears characteristics. For example, the large area of tears of non-visceral artery can be treated. As a result, the maximum distance between re-entry tears and the numbers of tears can be

**TABLE 1. Effects of changes in the number, maximum distance and area of re-entry tears on different hemodynamic parameters**

	Tear count	Tear maximum distance	Tear area
Flow field in FL	++	+	++
RRT < 1 area in FL	+	+++	++
OSI > 0.45 area	+++	–	++
ECAP > 1.5 area	+++	–	++
Low TAWSS between tears	++	+	++
Pressure difference between TL and FL	+	+++	+
Total “+” number	12	8	11

The number of “+” represents the varying degrees of influence on the hemodynamic environment in preventing thrombosis in FL in all three groups, with a higher number of “+” indicating a greater effect; “–” represents negative impact, *FL* represents false lumen, *RRT* represents relative residence time, *OSI* represents the oscillatory shear index, *ECAP* represents the endothelial cell activation potential, *TAWSS* represents the time-averaged wall shear stress.

also decreased following the partial distal tears repairment.

## CONCLUSIONS

Based on CFD simulation, this article revealed the correlation between the characteristics of re-entry tears and the potential thrombosis in the FL of TBAD patients following TEVAR. It was found that the count, maximum distance and area of re-entry tears could play an important role in determining hemodynamic factors that may influence thrombosis in FL after TEVAR and the tear count was the most crucial factor.

## LIMITATION

1. Although this study found that the parameters of re-entry tears have a great different influence on the tendency to thrombosis in the FL, we did not apply the CFD on the real models of patients, and the effect of the re-entry tear in the real physiological situation is worthy of further exploration.
2. Although some studies suggested that the difference of wall shear stress-related parameters between the fluid-structure interaction and rigid wall models was marginal,<sup>26</sup> some other researches showed that the change of wall shear stress was significant.<sup>18</sup> Therefore, how the aortic wall elasticity affects the role of tear morphology on the false lumen thrombosis after TEVAR needs to be explored in the future study.
3. It has been pointed out that the tear area has an effect on the fluttering of intimal flap during the cardiac cycle.<sup>15</sup> A larger tear area increases the fluttering of intimal flap, leading to a large variation of the false lumen during the cardiac

cycle. It is worth further investigation whether the increased fluttering of intimal flap will affect the thrombosis in the false lumen.

## SUPPLEMENTARY INFORMATION

The online version contains supplementary material available at <https://doi.org/10.1007/s13239-021-00532-z>.

## AUTHOR CONTRIBUTIONS

LD: Conceptualization, Software, Data Curation, Writing—Original Draft. YD: Resources, Software, Validation. LZ: Data curation, Software, Visualization. LY: Data Curation, Investigation. ZT: Conceptualization, Supervision, Writing - Review & Editing. FY: Project administration, Writing—Review & Editing.

## CONFLICT OF INTEREST

No conflict of interest.

## REFERENCES

- <sup>1</sup>Ab Naim, W. N. W., P. B. Ganesan, Z. H. Sun, Y. M. Liew, Y. Qian, C. J. Lee, *et al.* Prediction of thrombus formation using vortical structures presentation in Stanford type B aortic dissection: a preliminary study using CFD approach. *Appl. Math. Model.* 40(4):3115–3127, 2016. <https://doi.org/10.1016/j.apm.2015.09.096>.
- <sup>2</sup>Alimohammadi, M., O. Agu, S. Balabani, and V. Diaz-Zuccarini. Development of a patient-specific simulation tool to analyse aortic dissections: assessment of mixed patient-specific flow and pressure boundary conditions. *Med. Eng. Phys.* 36(3):275–284, 2014. <https://doi.org/10.1016/j.medengphy.2013.11.003>.

- <sup>3</sup> Armour, C. H., C. Menichini, K. Milinis, R. G. J. Gibbs, and X. Y. Xu. Location of reentry tears affects false lumen thrombosis in aortic dissection following TEVAR. *J. Endovasc. Ther.* 27(3):396–404, 2020. <https://doi.org/10.1177/1526602820917962>.
- <sup>4</sup> Ben Ahmed, S., D. Dillon-Murphy, and C. A. Figueroa. Computational study of anatomical risk factors in idealized models of type B aortic dissection. *Eur. J. Vasc. Endovasc. Surg.* 52(6):736–745, 2016. <https://doi.org/10.1016/j.ejvs.2016.07.025>.
- <sup>5</sup> Boccadifuoco, A., A. Mariotti, S. Celi, N. Martini, and M. V. Salvetti. Impact of uncertainties in outflow boundary conditions on the predictions of hemodynamic simulations of ascending thoracic aortic aneurysms. *Comput. Fluids.* 165:96–115, 2018. <https://doi.org/10.1016/j.compfluid.2018.01.012>.
- <sup>6</sup> Buck, A. K. W., J. J. Groszek, D. C. Colvin, S. B. Keller, C. Kensing, R. Forbes, et al. Combined in silico and in vitro approach predicts low wall shear stress regions in a hemofilter that correlate with thrombus formation in vivo. *ASAIO J.* 64(2):211, 2018.
- <sup>7</sup> Clough, R. E., D. Barilla, P. Delsart, G. Ledieu, R. Spear, S. Crichton, et al. Editor's choice—long-term survival and risk analysis in 136 consecutive patients with type B aortic dissection presenting to a single centre over an 11 year period. *Eur. J. Vasc. Endovasc.* 57(5):633–638, 2019. <http://doi.org/10.1016/j.ejvs.2018.08.042>.
- <sup>8</sup> Conrad, M. F., R. S. Crawford, C. J. Kwolek, D. C. Brewster, T. J. Brady, and R. P. Cambria. Aortic remodeling after endovascular repair of acute complicated type B aortic dissection. *J. Vasc. Surg.* 50(3):510–517, 2009. <http://doi.org/10.1016/j.jvs.2009.04.038>.
- <sup>9</sup> Czerny, M., J. Schmidli, S. Adler, J. C. van den Berg, L. Bertoglio, T. Carrel, et al. Current options and recommendations for the treatment of thoracic aortic pathologies involving the aortic arch: an expert consensus document of the European Association for Cardio-Thoracic surgery (EACTS) and the European Society for Vascular Surgery (ESVS). *Eur. J. Cardio-Thorac.* 55(1):133–162, 2019. <http://doi.org/10.1093/ejcts/ezy313>.
- <sup>10</sup> Dai, W. F., P. Wu, and G. M. Liu. A two-phase flow approach for modeling blood stasis and estimating the thrombosis potential of a ventricular assist device. *Int. J. Artif. Org.* 2020. <https://doi.org/10.1177/0391398820975405>.
- <sup>11</sup> Karmonik, C., J. Bismuth, M. G. Davies, D. J. Shah, H. K. Younes, and A. B. Lumsden. A computational fluid dynamics study pre- and post-stent graft placement in an acute type B aortic dissection. *Vasc. Endovasc. Surg.* 45(2):157–164, 2011. <https://doi.org/10.1177/1538574410389342>.
- <sup>12</sup> Karmonik, C., M. Muller-Eschner, S. Partovi, P. Geisbusch, M. K. Ganten, J. Bismuth, et al. Computational fluid dynamics investigation of chronic aortic dissection hemodynamics versus normal aorta. *Vasc. Endovasc. Surg.* 47(8):625–631, 2013. <https://doi.org/10.1177/1538574413503561>.
- <sup>13</sup> Kazimierczak, A., P. Rynio, T. Jedrzejczak, K. Mokrzycki, R. Samad, M. Brykczynski, et al. Expanded Petticoat technique to promote the reduction of contrasted false lumen volume in patients with chronic type B aortic dissection. *J. Vasc. Surg.* 2019. <https://doi.org/10.1016/j.jvs.2019.01.073>.
- <sup>14</sup> Kelsey, L. J., J. T. Powell, P. E. Norman, K. Miller, and B. J. Doyle. A comparison of hemodynamic metrics and intraluminal thrombus burden in a common iliac artery aneurysm. *Int. J. Numer. Methods Biol.* 33(5):2821, 2017. <https://doi.org/10.1002/cnm.2821>.
- <sup>15</sup> Keramati, H., E. Birgersson, J. P. Ho, S. Kim, K. J. Chua, and H. L. Leo. The effect of the entry and re-entry size in the aortic dissection: a two-way fluid–structure interaction simulation. *Biomech. Model. Mechanobiol.* 19(6):2643–2656, 2020. <https://doi.org/10.1007/s10237-020-01361-0>.
- <sup>16</sup> Li, D., L. Peng, Y. Wang, J. Zhao, D. Yuan, and T. Zheng. Predictor of false lumen thrombosis after thoracic endovascular aortic repair for type B dissection. *J. Thorac. Cardiovasc. Surg.* 160(2):360–367, 2020. <https://doi.org/10.1016/j.jtcvs.2019.07.091>.
- <sup>17</sup> Mao, W., Q. Wang, S. Kodali, and W. Sun. Numerical parametric study of paravalvular leak following a transcatheter aortic valve deployment into a patient-specific aortic root. *J. Biomechan. Eng.* 140(10):2018. <https://doi.org/10.1115/1.4040457>.
- <sup>18</sup> Mendez, V., M. Di Giuseppe, and S. Pasta. Comparison of hemodynamic and structural indices of ascending thoracic aortic aneurysm as predicted by 2-way FSI, CFD rigid wall simulation and patient-specific displacement-based FEA. *Comput. Biol. Med.* 100:221–229, 2018. <https://doi.org/10.1016/j.compbiomed.2018.07.013>.
- <sup>19</sup> Menichini, C., Z. Cheng, R. G. J. Gibbs, and X. Y. Xu. A computational model for false lumen thrombosis in type B aortic dissection following thoracic endovascular repair. *J. Biomech.* 66:36–43, 2018. <https://doi.org/10.1016/j.jbiomech.2017.10.029>.
- <sup>20</sup> Menichini, C., and X. Y. Xu. Mathematical modeling of thrombus formation in idealized models of aortic dissection: initial findings and potential applications. *J. Math. Biol.* 73(5):1205–1226, 2016. <https://doi.org/10.1007/s00285-016-0986-4>.
- <sup>21</sup> Munshi, B., L. P. Parker, P. E. Norman, and B. J. Doyle. The application of computational modeling for risk prediction in type B aortic dissection. *J. Vasc. Surg.* 71(5):1789, 2020. <https://doi.org/10.1016/j.jvs.2019.09.032>.
- <sup>22</sup> Nakatamari, H., T. Ueda, F. Ishioka, B. Raman, K. Kurihara, G. D. Rubin, et al. Discriminant analysis of native thoracic aortic curvature: risk prediction for endoleak formation after thoracic endovascular aortic repair. *J. Vasc. Interv. Radiol.* 22(7):974–979, 2011. <https://doi.org/10.1016/j.jvir.2011.02.031>.
- <sup>23</sup> Nienaber, C. A., and K. A. Eagle. Aortic dissection: New frontiers in diagnosis and management—part I: from etiology to diagnostic strategies. *Circulation.* 108(5):628–635, 2003. <https://doi.org/10.1161/01.Cir.0000087009.16755.E4>.
- <sup>24</sup> Nienaber, C. A., H. Rousseau, H. Eggebrecht, S. Kische, R. Fattori, T. C. Rehders, et al. Randomized comparison of strategies for type B aortic dissection the investigation of STent grafts in aortic dissection (INSTEAD) trial. *Circulation.* 120(25):2519–2528, 2009. <https://doi.org/10.1161/Circulationaha.109.886408>.
- <sup>25</sup> Pellenc, Q., A. Roussel, R. De Blic, A. Girault, P. Cerceau, L. Ben Abdallah, et al. False lumen embolization in chronic aortic dissection promotes thoracic aortic remodeling at midterm follow-up. *J. Vasc. Surg.* 70(3):710–717, 2019. <https://doi.org/10.1016/j.jvs.2018.11.038>.
- <sup>26</sup> Qiao, Y. H., Y. J. Zeng, Y. Ding, J. R. Fan, K. Luo, and T. Zhu. Numerical simulation of two-phase non-Newtonian blood flow with fluid–structure interaction in aortic dissection. *Comput. Method Biomech.* 22(6):620–630, 2019. <https://doi.org/10.1080/10255842.2019.1577398>.

- <sup>27</sup>Qiu, Y., Y. Wang, Y. B. Fan, L. Q. Peng, R. Liu, J. C. Zhao, *et al.* Role of intraluminal thrombus in abdominal aortic aneurysm ruptures: a hemodynamic point of view. *Med. Phys.* 46(9):4263–4275, 2019. <https://doi.org/10.1002/mp.13658>.
- <sup>28</sup>Qiu, Y., D. Yuan, Y. Wang, J. Wen, and T. H. Zheng. Hemodynamic investigation of a patient-specific abdominal aortic aneurysm with iliac artery tortuosity. *Comput. Method Biomech.* 21(16):824–833, 2018. <https://doi.org/10.1080/10255842.2018.1522531>.
- <sup>29</sup>Ruel, J., and G. Lachance. Mathematical modeling and experimental testing of three bioreactor configurations based on windkessel models. *Heart Int.* 5(1):2010. <https://doi.org/10.4081/hi.2010.e1>.
- <sup>30</sup>Ryzhakov, P., E. Soudah, and N. Dialami. Computational modeling of the fluid flow and the flexible intimal flap in type B aortic dissection via a monolithic arbitrary Lagrangian/Eulerian fluid-structure interaction model. *Int. J. Numer. Method Biomed. Eng.* 35(11):2019. <https://doi.org/10.1002/cnm.3239>.
- <sup>31</sup>Schwein, A., M. Khan, M. Bennett, N. Chakfe, A. B. Lumsden, J. Bismuth, *et al.* Proposed magnetic resonance imaging criteria to diagnose intramural haematoma and to predict aortic healing after acute type b aortic syndrome. *Eur. J. Vasc. Endovasc.* 57(3):350–359, 2019. <https://doi.org/10.1016/j.ejvs.2018.09.017>.
- <sup>32</sup>Sengupta, D., A. M. Kahn, E. Kung, M. E. Moghadam, O. Shirinsky, G. A. Lyskina, *et al.* Thrombotic risk stratification using computational modeling in patients with coronary artery aneurysms following Kawasaki disease. *Biomech. Model Mech.* 13(6):1261–1276, 2014. <https://doi.org/10.1007/s10237-014-0570-z>.
- <sup>33</sup>Sheriff, J., D. Bluestein, G. Girdhar, and J. Jesty. High-shear stress sensitizes platelets to subsequent low-shear conditions. *Ann. Biomed. Eng.* 38(4):1442–1450, 2010. <https://doi.org/10.1007/s10439-010-9936-2>.
- <sup>34</sup>Spinelli, D., F. Benedetto, R. Donato, G. Piffaretti, M. M. Marrocco-Trischitta, H. J. Patel, *et al.* Current evidence in predictors of aortic growth and events in acute type B aortic dissection. *J. Vasc. Surg.* 68(6):1925, 2018. <https://doi.org/10.1016/j.jvs.2018.05.232>.
- <sup>35</sup>Tsai, T. T., A. Evangelista, C. A. Nienaber, T. Myrmel, G. Meinhardt, J. V. Cooper, *et al.* Partial thrombosis of the false lumen in patients with acute type B aortic dissection. *N. Engl. J. Med.* 357(4):349–359, 2007. <https://doi.org/10.1056/NEJMoA063232>.
- <sup>36</sup>Vergara, C., F. Viscardi, L. Antiga, and G. B. Luciani. Influence of bicuspid valve geometry on ascending aortic fluid dynamics: a parametric study. *Artif. Org.* 36(4):368–378, 2012. <https://doi.org/10.1111/j.1525-1594.2011.01356.x>.
- <sup>37</sup>Wan Ab Naim, W. N., P. B. Ganesan, Z. Sun, J. Lei, S. Jansen, S. A. Hashim, *et al.* Flow pattern analysis in type B aortic dissection patients after stent-grafting repair: comparison between complete and incomplete false lumen thrombosis. *Int. J. Numer. Method Biomed. Eng.* 34(5):2018. <https://doi.org/10.1002/cnm.2961>.
- <sup>38</sup>Wan Ab Naim, W. N., P. B. Ganesan, Z. Sun, K. Osman, and E. Lim. The impact of the number of tears in patient-specific stanford type B aortic dissecting aneurysm: Cfd simulation. *J. Mech. Med. Biol.* 14(02):1450017, 2014. <https://doi.org/10.1142/s0219519414500171>.
- <sup>39</sup>Wang, H. R., H. Anzai, Y. J. Liu, A. K. Qiao, J. S. Xie, and M. Ohta. Hemodynamic-based evaluation on thrombosis risk of fusiform coronary artery aneurysms using computational fluid dynamic simulation method. *Complexity.* 2020. <https://doi.org/10.1155/2020/8507273>.
- <sup>40</sup>Wojtaszek, M., E. Wnuk, R. Maciag, K. Lamparski, K. Korzeniowski, and O. Rowinski. Promoting false-lumen thrombosis after thoracic endovascular aneurysm repair in type B aortic dissection by selectively excluding false-lumen distal entry tears. *J. Vasc. Interv. Radiol.* 28(2):168–175, 2017. <https://doi.org/10.1016/j.jvir.2016.07.007>.
- <sup>41</sup>Xiao, N., J. Alastruey, and C. Figueroa. A systematic comparison between 1-D and 3-D hemodynamics in compliant arterial models. *Int. J. Numer. Methods Biomed. Eng.* 30(2):204–231, 2014.
- <sup>42</sup>Xu, H., M. Piccinelli, B. G. Leshnower, A. Lefieux, W. R. Taylor, and A. Veneziani. Coupled Morphological-hemodynamic computational analysis of type B aortic dissection: a longitudinal study. *Ann. Biomed. Eng.* 46(7):927–939, 2018. <https://doi.org/10.1007/s10439-018-2012-z>.
- <sup>43</sup>Zhang, S. M., Y. Q. Chen, Y. X. Zhang, D. C. Shi, Y. Shen, J. M. Bao, *et al.* Should the distal tears of aortic dissection be treated? The risk of distal tears after proximal repair of aortic dissection. *Int. J. Cardiol.* 261:162–166, 2018. <https://doi.org/10.1016/j.ijcard.2018.01.028>.
- <sup>44</sup>Zhu, C., B. Huang, J. Zhao, Y. Ma, D. Yuan, Y. Yang, *et al.* Influence of distal entry tears in acute type B aortic dissection after thoracic endovascular aortic repair. *J. Vasc. Surg.* 66(2):375–385, 2017. <https://doi.org/10.1016/j.jvs.2016.12.142>.

**Publisher's Note** Springer Nature remains neutral with regard to jurisdictional claims in published maps and institutional affiliations.